RSC Advances

PAPER

Cite this: *RSC Adv.*, 2019, **9**, 12384

Forsythiaside inhibited titanium particle-induced inflammation *via* the NF-κB signaling pathway and RANKL-induced osteoclastogenesis and titanium particle-induced periprosthetic osteolysis *via* JNK, p38, and ERK signaling pathways

Kaihang Xu, †[a] Rongzhi He,†[a] Yuan Zhang,†[b] Sheng Qin,[a] Guangchao Wang,[a] Qiang Wei,[a] Hao Zhang*[a] and Fang Ji*[a]

Wear particle-induced periprosthetic osteolysis is the primary complication of the total joint replacement; however, no conservative treatment except for reversal surgery is available for this disease. During the past decade, Chinese herbal medicines have been widely investigated to inhibit osteoclast differentiation, which may exhibit the potential to treat wear particle-induced periprosthetic osteolysis. The present study was aimed at the investigation of the effects of forsythiaside on osteocytes. The current data revealed that the forsythiaside treatment notably inhibited the titanium (Ti) particle-induced inflammation through impaired NF-κB signaling, thereby inhibiting TNF-α and IL-1β. In addition, the *in vitro* study demonstrated that forsythiaside effectively prevented the RANKL-induced differentiation of osteoclasts and inhibited the expression of osteoclast-specific genes in osteoclasts *via* inhibition of the JNK signaling pathway. The *in vivo* study of Ti particle-induced implant-associated osteolysis indicated that forsythiaside could also inhibit osteoclastogenesis. In summary, forsythiaside could inhibit osteoclastogenesis and particle-induced inflammation, resulting in decreased secretion of inflammatory cytokines such as TNF-α and IL-1β. On the other hand, forsythiaside could inhibit RANKL-induced osteoclastogenesis and Ti particle-induced periprosthetic osteolysis *via* JNK, ERK and p38 signaling pathways. Both the abovementioned biofunctions of forsythiaside contributed to the implant-associated particle-induced osteolysis. Thus, forsythiaside can act as a candidate drug for the precaution of implant-associated particle-induced osteolysis.

Received 5th December 2018
Accepted 26th March 2019

DOI: 10.1039/c8ra10007a

rsc.li/rsc-advances

Introduction

With the aging population and the demand for high-quality life, the number of individuals that undergo arthroplasty is increasing since it is an effective treatment for severe trauma and arthritic joint diseases.[1] Due to their excellent biocompatibility, titanium (Ti) and its alloys have widespread applications in prostheses. However, aseptic prosthetic loosening, one of the long-term complications after joint arthroplasty, limits the longevity of the prostheses.[2] Wear particles, released from prosthetic implants, are speculated to play a crucial role as corrosive products and reactive oxygen species, which ultimately induce an inflammatory reaction;[3,4] currently, only a few drugs are available that can effectively treat or alleviate bone resorption surrounding the prosthetic implant and thus would aid in understanding the underlying formation mechanism and promoting the related functional studies.

T lymphocytes, fibroblasts, macrophages, and foreign body giant cells are stimulated by wear particles to produce a vast array of pro-inflammatory cytokines, which would induce the expression of RANKL by osteoblasts and marrow stromal cells.[5] Accumulating evidence has demonstrated that the formation of osteoclasts is mainly determined by two key factors, *i.e.*, macrophage colony-stimulating factor (M-CSF) and receptor activator for the nuclear factor-κB ligand (RANKL), which is the key factor for osteoclast differentiation.[6] During the activation of osteoclastogenesis, five signaling cascades mediated by protein kinases are activated: an inhibitor of NF-κB kinase (IKK), c-Jun N-terminal kinase (JNK), p38, extracellular signal-regulated kinase (ERK), and the Src pathway.[7,8] Numerous studies have described that the activation of the RANK and the

[a]*Department of Orthopedics, Changhai Hospital Affiliated to the Navy Military Medical University, Changhai Hospital, The Navy Military Medical University, No. 168 Changhai Road, Shanghai 200433, People's Republic of China. E-mail: zhanghsmmu@126.com; doctorjif@126.com; Fax: +86-021-31161682; +86-021-31161696; Tel: +86-021-31161682; +86-021-31161696*

[b]*Department of Ophthalmology, Changhai Hospital Affiliated to the Navy Military Medical University, Shanghai, People's Republic of China*

† These authors contributed equally to this article.

RANKL signaling pathways elevates osteoclastogenesis, which leads to osteolysis around the prosthesis.[9–11] Hence, targeting the osteoclastogenesis might be a promising approach for the treatment of periprosthetic osteolysis.

Several studies have focused on the use of Chinese herbs to inhibit osteoclast differentiation; for example, icariin prevents the Ti particle-induced inhibition of osteogenic differentiation in MSCs,[12] melatonin prevents Ti particle-induced inflammatory bone resorption and osteoclastogenesis *via* suppression of the NF-κB signaling and the activation of the Wnt/β-catenin signaling pathway,[13,14] and myricetin inhibits RANKL-induced osteoclastogenesis *in vitro* and prevents the Ti particle-induced osteolysis *in vivo*.[15] Thus, Chinese herbs might exhibit a great potential in the treatment of Ti particle-induced osteolysis.

Forsythiaside, a traditional Chinese medicine, is widely used for heat clearing and detoxification. It contains a variety of ester glycosides, of which, forsythiaside is an effective active ingredient.[16,17] In addition, it has a wide spectrum of properties along with robust antibacterial efficiency against *Staphylococcus aureus*.[18,19] Surprisingly, in our previous studies, we have found that forsythiaside exerts a significant inhibitory effect on osteoclast activity; although the inhibitory effect of forsythiaside on the osteoclast activity has been confirmed, the underlying mechanism of action and the *in vivo* effects are not yet clarified. In view of the bacterial erosion of postoperative bone infections and the pathological state of the massive activation of osteoclasts in an inflammatory environment, forsythiaside effectuates broad-spectrum antibacterial properties and the dual efficacy of inhibiting osteoclasts, thereby rendering it as an ideal drug for the prevention and treatment of post-plant infections.[20] Thus, we induced osteocyte apoptosis and investigated the effects of forsythiaside on apoptotic osteocytes and subsequent osteoclastogenesis *in vitro* and *in vivo*. Based on the results obtained herein, we speculated that forsythiaside might be a novel candidate for the treatment of periprosthetic osteolysis.

Material and methods

Materials

Titanium (Ti) particles (Johnson Matthey), mouse macrophage RAW264.7 cells (ATCC, American), alpha minimum essential medium (α-MEM; Hyclone), fetal bovine serum (FBS; Gibco, Australia), CCK-8 kit (Dongjido, Japan), trypsin–EDTA (0.5%), penicillin, streptomycin (Gibco, Australia), forsythiaside (Solarbio, China), Trizol reagents (Life Technologies, Australia), RNeasy Mini Kit (Qiagen). Trizol (Invitrogen), RIPA (Beyotime biotechnology), TRAP staining kit (Sigma), mouse RANKL and M-CSF (R&D), MAPK Family Antibody Sampler Kit and NF-κB Family Member Antibody Sampler Kit (Cell signaling technology), cDNA synthesis kit, real-time PCR kit (SYBR Premix EX Taq, TaKaRa), Pierce™ bicinchoninic acid (BCA) protein assay kit (ThermoFisher), and TNF-α ELASA kit and IL-1β ELISA kit (R&D).

Methods

BMM extraction and osteoclast differentiation. We isolated bone marrow-derived macrophages (BMMs) from the femur and tibia bone marrow of 5 week-old C57BL/6 mice. Freshly isolated BMMs were cultured in a T75 flask in α-MEM supplemented with 30 ng mL^{-1} macrophage colony-stimulating factor (M-CSF), 10% fetal bovine serum (FBS), and 1% penicillin/streptomycin for 24 h. The cells were cultured in an incubator maintained at 37.8 °C under 5% CO_2 atmosphere for 4 days until confluency. Consecutively, the non-adherent cells were removed from the culture.

Cell viability assay of forsythiaside on RAW 264.7 and cell apoptosis assay of forsythiaside on BMM cells. The effect of forsythiaside on the viability of RAW 264.7 was determined by the CCK-8 assay. Briefly, the RAW 264.7 cells were plated in 96-well plates at the density of 1×10^4 cells per well and cultured in a complete α-MEM medium containing forsythiaside at different concentrations (0, 10, 25, 50, and 100 μg mL^{-1}) for 24, 48, and 72 h. Next, 10 μL CCK-8 was added to each well, and the plates were incubated at 37 °C for an additional 2 h. Then, the optical density (OD) was measured using the ELX800 absorbance microplate reader (BioTek, Winooski, USA) at 450 nm (650 nm as a reference). After this, annexin V-FITC and PI staining (Thermo Fisher Scientific) were conducted according to the manufacturer's instructions. The BMM cells were seeded in 6-well plates at the density of 5000 cells per well. The cells were pretreated with a fresh medium with or without forsythiaside on the next day and harvested using 0.05% trypsin at 24, 48, and 72 h after initiation of the treatment, followed by staining with annexin V-FITC and PI according to the manufacturer's instructions. The cells were analyzed using a flow cytometer (USA) and FlowJo 10.2 software (Ashland, USA).

Tartrate-resistant acid phosphatase (TRAP) staining and resorption pit assay. The BMM cells were seeded in a 96-well plate at the density of 8×10^3 cells per well in complete α-MEM supplemented with 30 ng mL^{-1} M-CSF, 50 ng mL^{-1} RANKL, and forsythiaside at different concentrations (0, 25, or 50 μM). The culture medium was replaced every 2 days until mature osteoclasts had formed. The cells were fixed with 4% paraformaldehyde for 20 min and stained for TRAP using the Diagnostic Acid Phosphatase Kit. The TRAP-positive cells with more than three nuclei were counted as osteoclast-like cells. The BMM cells (2.4×10^4 cells per cm^2) were seeded on the bovine bone slices. After 48 h, the BMM cells were stimulated with 50 ng mL^{-1} RANKL, 30 ng mL^{-1} M-CSF, and forsythiaside (0, 25, or 50 μM) until mature osteoclasts were formed. Then, the cells were removed by mechanical agitation and sonication. The resorption pits were visualized using a scanning electron microscope (SEM, FEI Quanta 250). Herein, three fields of view were randomly selected for each bone slice for further analysis, and the bone surface resorption area was quantified using the Image J software (National Institutes of Health, MD, USA).

RNA extraction and quantitative real-time PCR. We used quantitative real-time PCR to analyze the specific gene expression during osteoclast formation. The BMM cells obtained from the C57BL/6 mice were seeded in 24-well plates at the density of 1×10^5 cells per well. Then, the BMM cells were stimulated with RANKL, M-CSF, and different doses of forsythiaside (0, 25, or 50 μM) for 5 days. Following the manufacturer's instructions, RNA was extracted using TRIzol, and cDNA was reverse transcribed

from 1 mg of total RNA using reverse transcriptase. Real-time PCR was performed using SYBR1 Premix ExTaq™ II and the ABI 7500 Sequencing Detection System (Applied Biosystems, Foster City, CA, USA). The following cycling conditions were used: 40 cycles of denaturation at 95 °C for 5 s and amplification at 60 °C for 24 s. *GAPDH* served as a housekeeping gene. The mouse primer sequences for *TRAP*, cathepsin K (*CTSK*), calcitonin receptor (*CTR*), *V-ATPase-d2*, *V-ATPase-a3*, *NFATc1*, *DC-STAMP*, and *GAPDH* are listed in Table 1.

Western blotting. The RAW 264.7 cells were seeded in 6-well plates at the density of 6×10^5 cells per well and pretreated with or without forsythiaside (25 μM) for 10 min, 20 min, 30 min, and 1 h; then, they were stimulated with RANKL and M-CSF. When the osteoclasts had formed, we extracted total proteins from these cells using the radioimmunoprecipitation assay (RIPA) lysis buffer. The cells were then separated by sodium dodecyl sulfate-polyacrylamide gel electrophoresis (SDS-PAGE) and transferred to polyvinylidene difluoride (PVDF) membranes. Subsequently, the membranes were blocked with 5% skimmed milk in TBST for 1 h and probed with different antibodies, followed by incubation with appropriate HRP-conjugated secondary antibodies. Finally, according to the manufacturer's instructions, the membrane was developed by enhanced chemiluminescent (ECL) reagents and imaged using Image Quant LAS 4000 (GE Healthcare, Silverwater, Australia). Quantification was obtained from phosphorylated proteins as compared to the total proteins and then normalized to the control group.

Cell viability assay of forsythiaside on the THP-1 cell and inhibition of Ti particle-induced inflammation by forsythiaside. The human macrophage cell line THP-1 was obtained from the Chinese Academy of Sciences and cultured in an RPMI 1640 medium supplemented with 10% FBS at 37 °C in a humidified 5% CO_2 incubator. The THP-1-deprived macrophages were induced with phorbol myristate acetate (PMA) at the concentration of 100 ng mL^{-1} for 12 h. The effect of forsythiaside on the viability of THP-1-deprived macrophages was determined by the CCK-8 assay according to the previous method. Then, we determined the mRNA levels of inflammation-related and macrophage polarization-related genes, including *TNF-α* and *IL-1β*, on day 3 of the incubation of the THP-1-deprived macrophage in forsythiaside (50 μM)-treated groups as compared to those in the control group, Ti particle and forsythiaside and Ti particle co-treated group. Moreover, the inflammatory cytokine secretion was examined on day 3 of the culture with *TNF-α* and *IL-1β* ELISA kit. The IκBα and p-IκBα were also detected in forsythiaside and Ti particle co-treated groups as compared to the case of the Ti particle-treated group, forsythiaside (50 μM)-treated group and RANKL-treated group *via* western-blotting assay.

Table 1 Primers for osteoclast differentiation marker

Gene	Primer sequence
TRAP	(F) 5′-CTG GAG TGC ACG ATG CCA GCG ACA-3′
	(R) 5′-TCC GTG CTC GGC GAT GGA CCA GA-3′
CTSK	(F) 5′-CTT CCA ATA CGT GCA GCA GA-3′
	(R) 5′-TCT TCA GGG CTT TCT CGT TC-3′
CTR	(F) 5′-TGC AGA CAA CTC TTG GTT GG-3′
	(R) 5′-TCG GTT TCT TCT CCT CTG GA-3′
V-ATPase-d2	(F) 5′-AAG CCT TTG TTT GAC GCT GT-3′
	(R) 5′-TTC GAT GCC TCT GTG AGA TG-3′
V-ATPase-a3	(F) 5′-GCC TCA GGG GAA GGC CAG ATC G-3′
	(R) 5′-GGC CAC CTC TTC ACT CCG GAA-3′
NFATC1	(F) 5′-CCGTTGCTTCCAGAAAATAACA-3′
	(R) 5′-TGTGGGATGTGAACTCGGAA-3′
DC-STAMP	(F) 5′-AAA ACC CTT GGG CTG TTC TT-3′
GAPDH	(R) 5′-AAT CAT GGA CGA CTC CTT GG-3′
	(F) 5-ACCCAGAAGACTGTGGATGG-3
	(R) 5-CACATTGGGGGTAGGAACAC-3

Micro-computed tomography (CT) scanning, histological, and histomorphometry analysis. A particle-induced peri-implant-associated osteolysis rat model was established. Briefly, a Ti implant (1.5 mm × 10 mm) was implanted laterally into the femoral condyle, and then, Ti particles were injected into the tissue around the implant. After 4 weeks post-surgery, the rats were sacrificed, and femurs were harvested under sterile conditions. Next, a high-resolution micro-CT (Skyscan, Belgium) was employed to analyze the femoral condyle. The scanning protocol was set at the isometric resolution at 20 mm and X-ray energy settings of 80 kV and 80 mA. After reconstruction, a square region of interest (ROI) around the midline suture was selected for further qualitative and quantitative analyses. Bone volume/tissue volume (BV/TV), the number of porosities, and the percentage of total porosity of each sample were measured, as reported previously.

Statistical analysis. The obtained results were analyzed by the SPSS 13.0 software (IBM) and expressed as mean ± SD. $P < 0.05$ was considered as a significant difference between groups. The experiments were carried out at least three times.

Results

BMM cell viability and cytotoxicity assay for the effect of forsythiaside

The CCK-8 assay was used to determine the cell viability of forsythiaside on BMMs. As shown in Fig. 1, cell viability was not altered in the presence of <50 μM but was inhibited at 100 μM concentration of forsythiaside. To further examine the effect of forsythiaside on cell apoptosis, the BMM cells were incubated with various doses of the drug and stained with annexin V and PI. Furthermore, the drug at the dosage of 10–50 μM did not induce either necrosis or apoptosis pathways in the BMM cells (Fig. 1).

TRAP staining and bone slice resorption pit of forsythiaside-inhibited osteoclastogenesis *in vitro*

Next, we investigated the effect of forsythiaside on osteoclast formation *via* TRAP staining and bone slice resorption pit. BMMs were cultured in a 96-well plate and then treated with 30 ng mL^{-1} M-CSF and 50 ng mL^{-1} RANKL in the presence or absence of forsythiaside at different concentrations for 5 days. As shown in Fig. 2, a large number of TRAP-positive osteoclasts were formed in the blank group. However, the number of

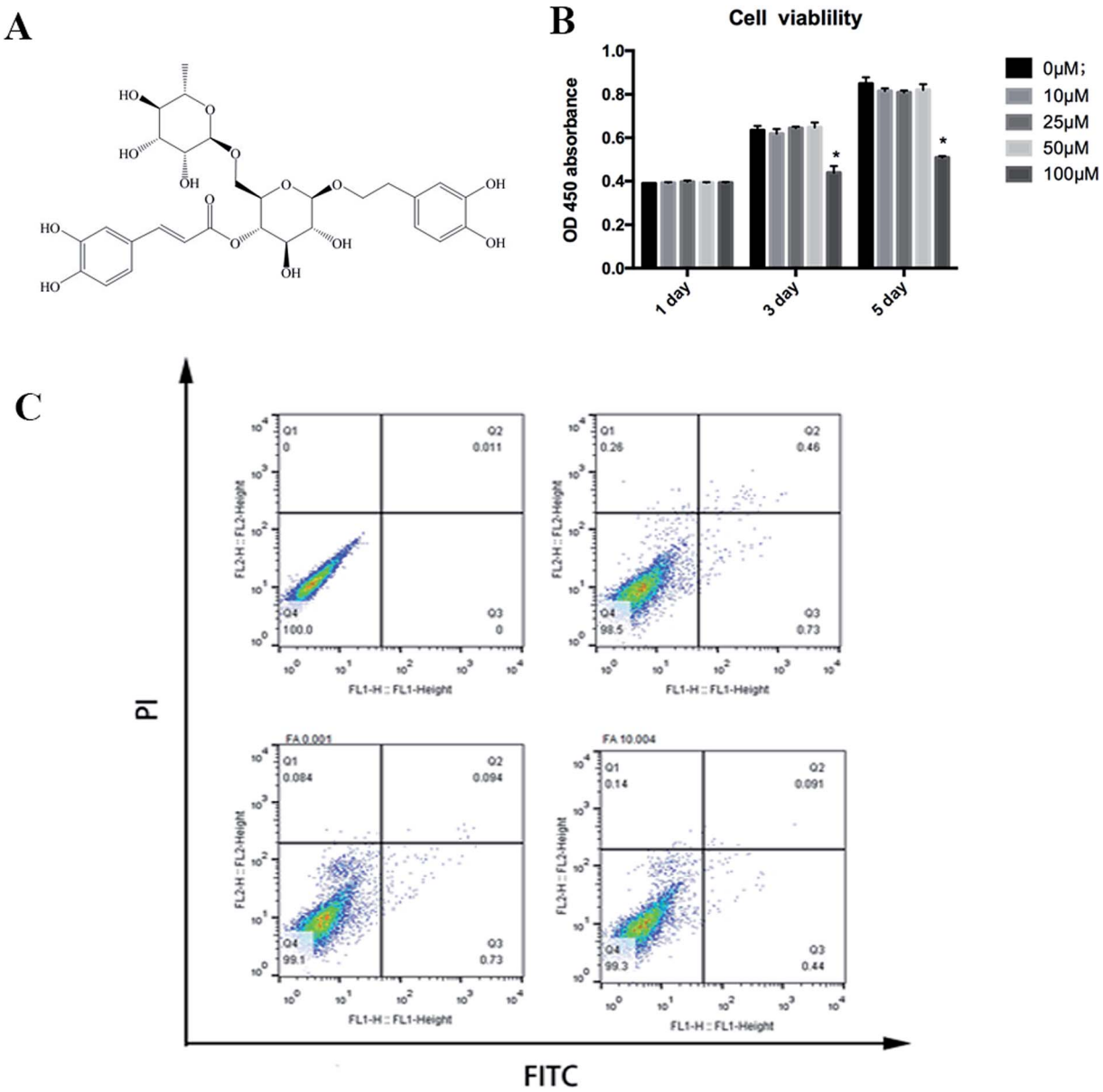

Fig. 1 (A) Chemical structure of forsythiaside. (B) Cell viability of forsythiaside after (C) Cell apoptosis of for sythiaside, *$P < 0.05$.

mature osteoclasts was significantly decreased in the forsythiaside-treated cells. Importantly, forsythiaside inhibited osteoclastogenesis in a dose-dependent manner. Approximately, 60% fewer TRAP-positive osteoclasts were observed in the cells treated with 50 μM forsythiaside (Fig. 2A).

Furthermore, we investigated the osteoclast bone resorption after the addition of forsythiaside at varying concentrations in the culture media for 5 days. Bone slices were selected and prepared for scanning electron microscopy (SEM). As shown in Fig. 2C and D, scattered bone resorption pits were observed on the surface of bone slices in the control group. On the other hand, the resorption area was decreased to 30% and <20% after treatment with 25 and 50 μM forsythiaside, respectively. Moreover, almost no resorption pits were observed in the slices treated with 50 μM forsythiaside. Thus, these findings suggested that forsythiaside impaired the osteoclast bone resorption *in vitro*.

Real-time PCR for the osteoclast differentiation of forsythiaside

Subsequently, we used quantitative PCR (qPCR) to analyze and quantify the RANKL-induced mRNA expression of osteoclast-related genes (including TRAP, *CTR*, *CTSK*, dendritic cell-specific transmembrane protein (*DC-STAMP*), *V-ATPase a3*, *V-ATPase d2*, and *NFATC1*) to confirm the inhibitory effects of forsythiaside on osteoclast formation. As shown in Fig. 3, the osteoclast-related gene expression was suppressed by forsythiaside in a dose-dependent manner. These data further confirmed that forsythiaside suppressed the osteoclast

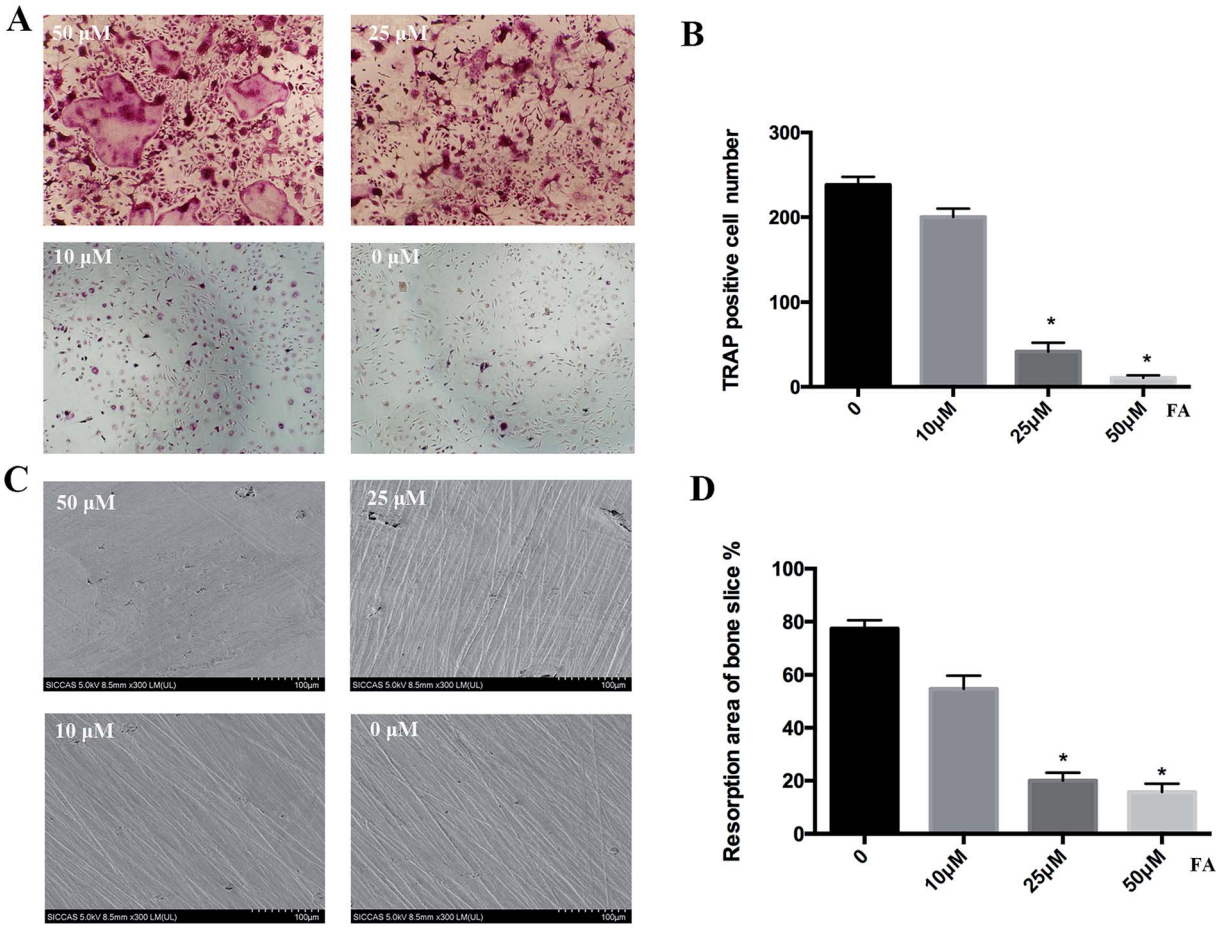

Fig. 2 Forsythiaside inhibited the RANKL-induced osteoclastogenesis at specific concentrations. (A) BMMs were treated with the indicated concentrations of forsythiaside and then with 30 ng mL^{-1} M-CSF and 50 ng mL^{-1} RANKL for 5 days. Cells were fixed with 4% (w/v) paraformaldehyde and stained for TRAP. (B) The number of TRAP (+) cells. (C) Representative scanning electron microscopy (SEM) images of bone-resorption pits are shown. (D) The total area of resorption pits, measured using Image J. Similar results were obtained (*$P < 0.05$). FA denotes forsythiaside.

formation and inhibited the expression of the osteoclast-specific genes.

Western-blotting for the investigation of the ERK, JNK, p38 signaling pathways

Western blotting was employed to investigate the potential signaling pathways underlying the osteoclast differentiation after forsythiaside intervention. The RAW264.7 cells were treated with RANKL in the presence or absence of forsythiaside, and then, the JNK, ERK, and p38 signaling pathways were examined using specific antibodies. The phosphorylation of JNK, ERK, and p38 was increased within 10–60 min after stimulation with RANKL in the control group. However, the ERK, JNK, and p38 phosphorylations were significantly inhibited after the treatment of cells with forsythiaside and after stimulation with RANKL and forsythiaside (Fig. 4). The total protein ERK1/2 was different at 10 minutes, 20 minutes, and 30 minutes. Although there was no significant difference in p-ERK1/2, the quantitative data showed a difference when the data obtained at 10 min, 20 min, and 30 min were compared (Fig. 4). A significant difference in p-JNK/JNK appeared at 10 min and 60 min, and a substantial change in p-p38/p38 appeared at 20 min and 30 min (Fig. 4). Altogether, these data suggested that forsythiaside inhibited osteoclastogenesis by primarily targeting the ERK, JNK, and p38 signaling pathways.

Inhibition of Ti particle-induced inflammation

The CCK-8 assay was used to determine the cell viability of forsythiaside on THP-1. Fig. 5E demonstrates that the THP-1 cell viability has not been affected in the presence of forsythiaside at <50 μM. We determined the mRNA levels of inflammation-related and macrophage polarization-related genes, including *TNF-α* and *IL-1β*, on day 3 of incubation in the forsythiaside-treated groups as compared to those in the control group (Fig. 5A and B). Moreover, the inflammatory cytokine secretion was examined on day 3 of culture. The expression of the inflammatory cytokines TNF-α and IL-1β decreased in the presence of forsythiaside at low or high concentrations (Fig. 5C and D); this demonstrated that macrophages in contact with Ti particles triggered an inflammatory

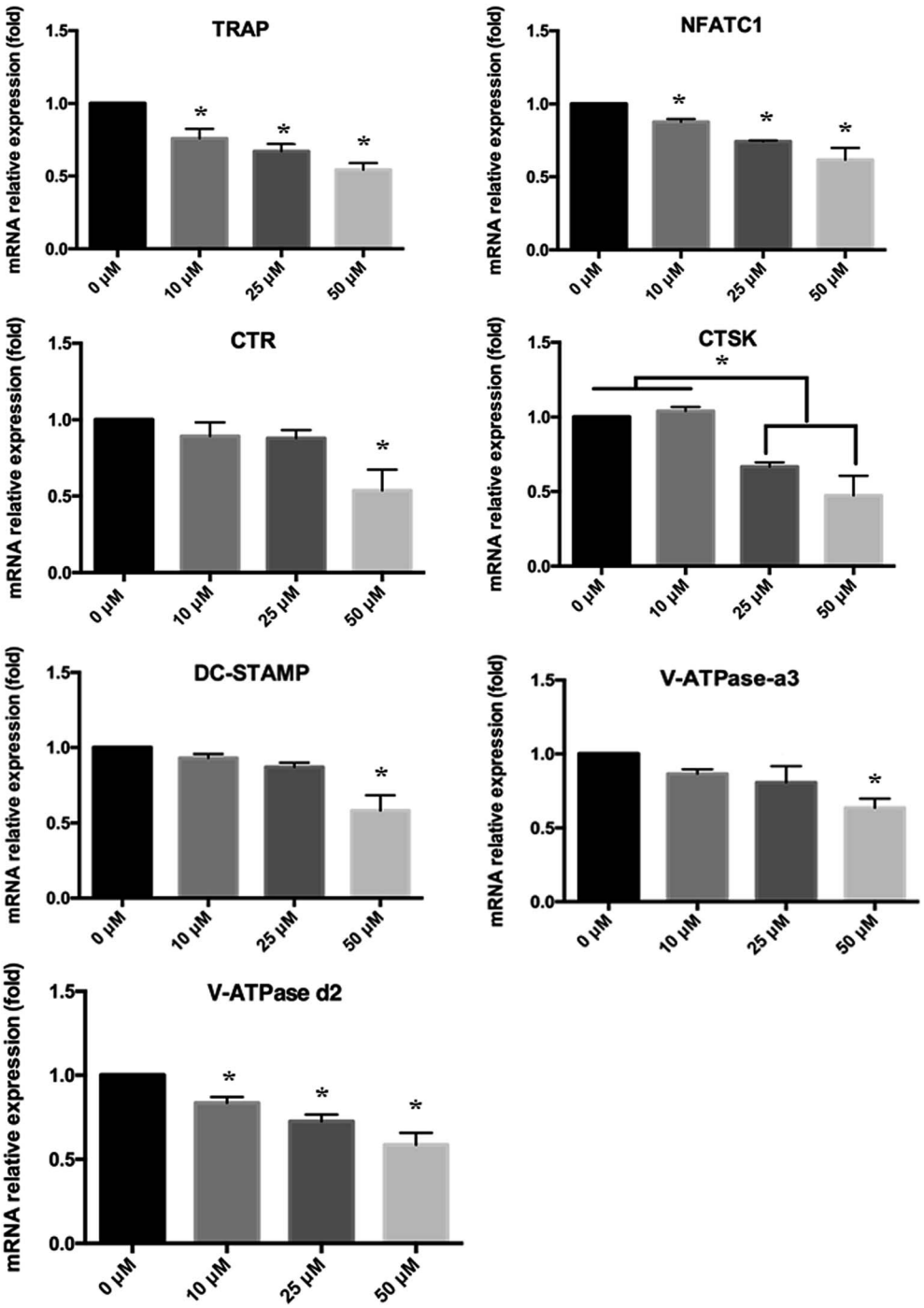

Fig. 3 Real-time PCR for the characterization of osteoclast differentiation-related genes such as *TRAP*, *NFATc1*, *CTR*, *CTSK*, *DC-STAMP*, *V-ATPase-a3*, and *V-ATPase-d2* (*$P < 0.05$ as compared to the blank group).

microenvironment that increased the infiltration of macrophages and the release of inflammatory mediators. On the other hand, the addition of forsythiaside inhibited the expression of *TNF-α* and *IL-1β* genes and the release of *TNF-α* and *IL-1β* inflammatory cytokines. Furthermore, western blotting demonstrated that forsythiaside administration decreased the NF-κB activation and the levels of p-IκBα; this, in turn, increased the production of the inhibitor of NF-κB (IκBα) and inhibited the downstream activation of NF-κB and the secretion of inflammatory cytokines, TNF-α and IL-1β. The FA + Ti particles at 30 min obviously provided highest p-IKB-alpha; this suggested that the highest NFκB signaling levels mainly resulted from the Ti particles (Fig. 5F). However, after 15 min, the p-IKB-alpha significantly reduced; this suggested the reduction of the NFκB signaling levels. We speculated that forsythiaside might have a delayed effect on the NFκB signaling levels.

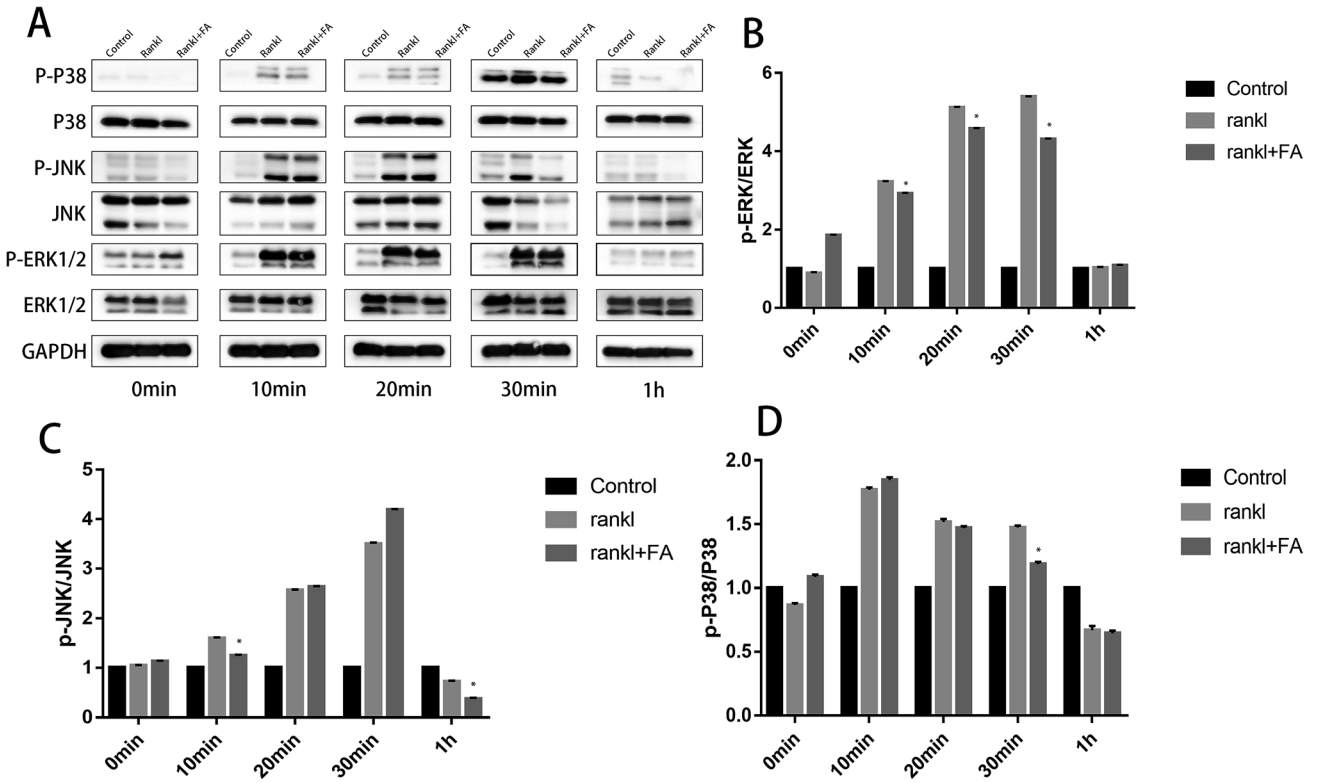

Fig. 4 Forsythiaside inhibited osteoclast differentiation by specifically impairing the RANKL-induced MAPK (p38, JNK, and ERK) cascades (*P < 0.05). (A): p38, JNK, and ERK were determined with western-blotting. (B) p-ERK/ERK was quantified and normalized to GAPDH. (C) p-JNK/JNK was quantified and normalized to GAPDH. (D): p-p38/p38 was quantified and normalized to GAPDH (*P < 0.05). * means comparison between RANKL + FA comparing to RANKL. FA denotes forsythiaside.

Micro-CT for the characterization of Ti particle-induced osteolysis

The effect of forsythiaside on Ti particle-induced implant-associated osteolysis was examined in a SD rat model. Micro-CT with three-dimensional reconstruction revealed an extensive bone resorption in the Ti particle group. In the groups with forsythiaside intervention, particle-induced implant-associated osteolysis was inhibited in a dose-dependent manner, whereas bone resorption in mice treated with forsythiaside at high concentrations was much lower than that at low concentrations. BV/TV, the number of porosities, and the percentage of total porosity in the ROI were measured based on the three-dimensional reconstruction images as reported previously. Compared to the case of the sham control, the presence of Ti particles induced significant osteolysis in the implant around the bone tissue (Fig. 6). When forsythiaside was injected at 5 mg kg^{-1} and 10 mg kg^{-1} daily, the osteolytic bone loss was prevented as compared to the case of the Ti particle group.

Discussion

Orthopedic implant-associated osteolysis is the primary drawback of implant failure in the long-term, especially with respect to the prosthetic replacement. Although the pathogenesis of the orthopedic implant-associated osteolysis is widely investigated, no efficient clinical measure is yet available.[21]

Several factors contribute to the process of implant-associated osteolysis.[22] In addition, the cytokines of the innate immune system play a vital role in the pathology of orthopedic implant failure.[23,24] The basic biological mechanism of aseptic loosening includes the stimulation of the wear particles on the surrounding macrophages to produce a series of inflammatory factors (TNF-α, IL-1β, and IL-6) upon chronic inflammation; these inflammatory factors can stimulate the osteoclast differentiation and maturation. In addition, the osteogenic differentiation and function are inhibited, and the inflammatory cells accumulate in the lesion, exerting a cascade effect, eventually causing osteolysis around the implant. As described previously, forsythiaside inhibited the LPS-induced inflammatory factors IL-6, IL-1β, and TNF-α and the production of Cox-2 *via* the inactivation of NF-κB.[25] Furthermore, forsythiaside attenuated the Ti-induced activation of NF-κB signaling, targeting the IκB kinase-α (IKKα) of macrophages and influencing the expression of NF-κB downstream inflammatory cytokines.[26]

On the other hand, excessive osteoclast differentiation, originating from the wear particles, plays a critical role in the process of osteoclastogenesis. RANKL-induced osteoclastogenesis is the main pathway in the formation of mature osteoclasts. After RANKL binds to RANK, the downstream cascade of TRAF-6 and TAK1 is activated; moreover, the activated TAK1 phosphorylates both IκB kinase (IKK) and MAPK kinases (MKKs); this, in turn, stimulates the NF-κB and MAPK signaling pathways, critical for osteoclastogenesis.[27] In the present study,

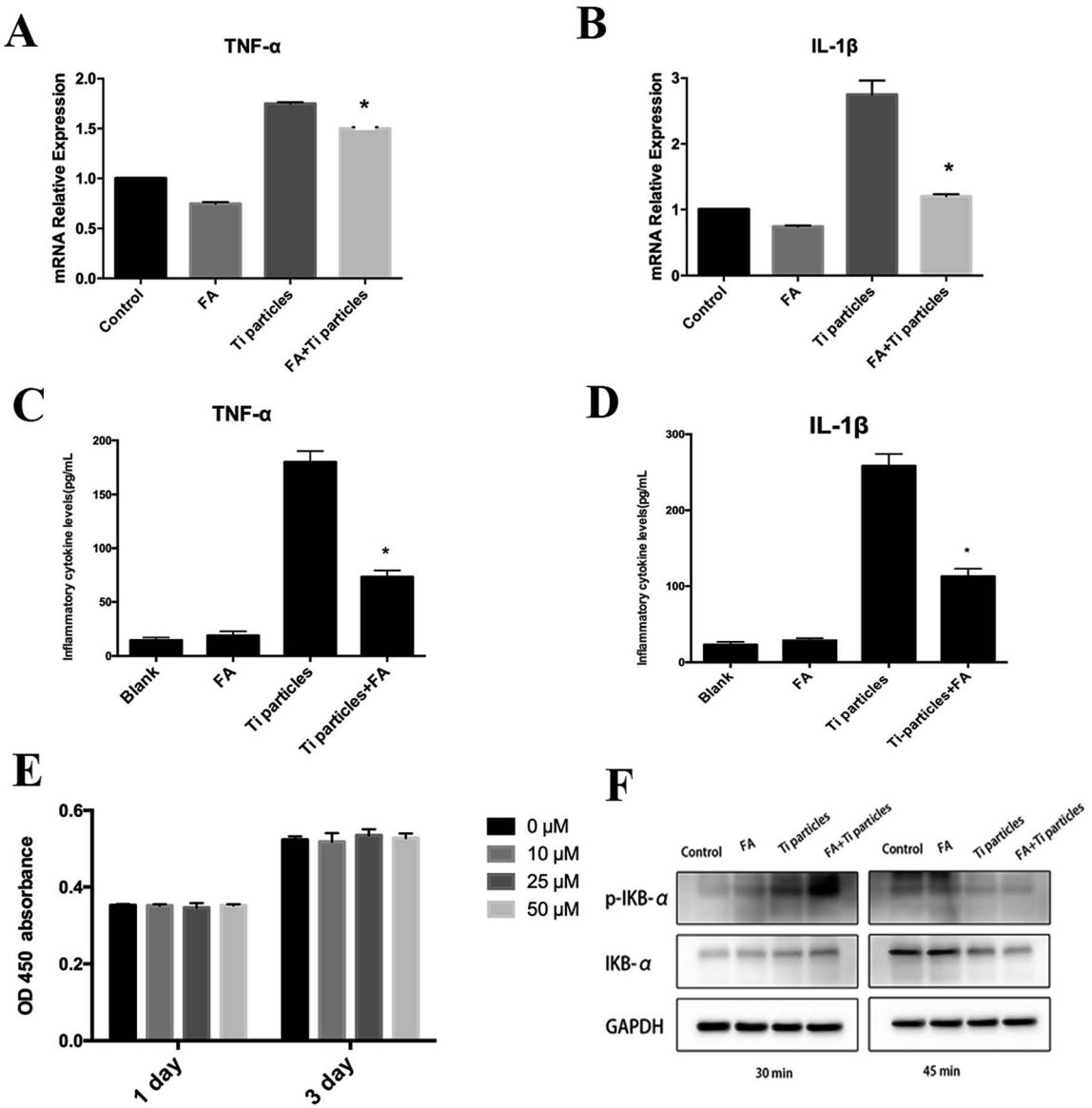

Fig. 5 Forsythiaside inhibited Ti particles-induced inflammation. (A and B) Real-time PCR for the determination of inflammation-related gene expression. (C and D) TNF-α and IL-1β secretion after the co-culture of particles with THP-1 cells. (E) Cell viability of forsythiaside on THP-1. (F) Proteins were extracted after the co-culture of particles with THP-1 cells, and the NF-κB signaling pathway was characterized by western blotting (*$P < 0.05$). FA denote forsythiaside.

forsythiaside inhibited the RANKL-induced osteoclastogenesis and Ti particle-induced periprosthetic osteolysis *via* JNK signaling.

Wear debris upregulated the various pro-inflammatory cytokines and chemokines in a range of cell types such as macrophages, osteoclast precursor cells, osteoblasts, and lymphocytes, which were at the interface between the implants and the surrounding bone. Together, these cells could affect the other cells through distinct signaling mechanisms. The inflammatory environment would accelerate osteoclast differentiation. Thus, the ideal target of inhibition of wear particles associated osteolysis including the inhibition of particles-induced inflammation; RANKL-induced osteoclastogenesis and Ti particle-induced periprosthetic osteolysis. In the present study, forsythiaside inhibited the Ti particle-induced inflammation *via* NF-κB signaling pathway and RANKL-induced osteoclastogenesis and Ti particle-induced periprosthetic osteolysis *via* JNK signaling pathways.

In summary, forsythiaside could inhibit osteoclastogenesis while inhibiting the particle-induced inflammation, resulting in decreased secretion of inflammatory cytokines, such as TNF-α, IL-1β, and inhibited the TNF-α-, IL-1β-induced osteoclastogenesis. On the other hand, forsythiaside inhibited the RANKL-induced osteoclastogenesis and Ti particle-induced periprosthetic osteolysis *via* JNK signaling pathway. Both the abovementioned biofunctions of forsythiaside contributed to the implant-associated particle-induced osteolysis. Thus, forsythiaside can act as a candidate for the precaution of implant-associated particle-induced osteolysis.

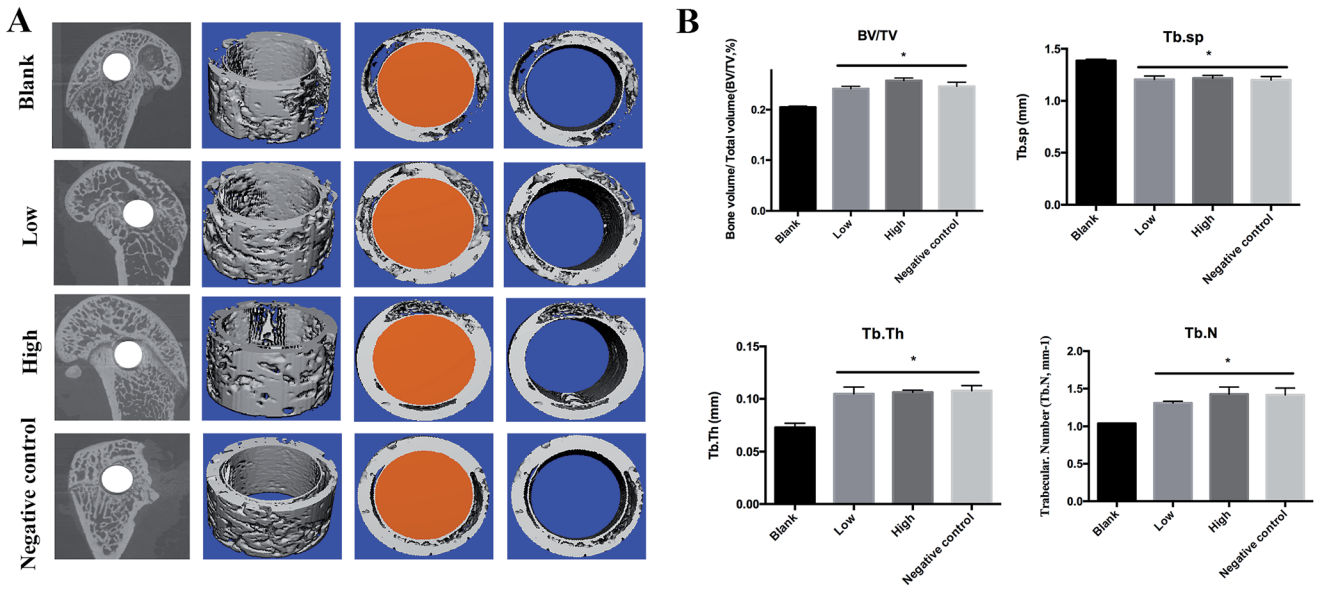

Fig. 6 Forsythiaside inhibited the implant-associated osteolysis *in vivo*. Ti implant (1.5 mm × 10 mm) was implanted into the femoral condyle, and then, Ti particles were injected into the tissue around the implant. After that, forsythiaside or PBS was injected every alternate day for 14 days. At the end, all mice were sacrificed, and the femurs were excised. (A) Representative micro-CT 3D reconstructed images were obtained for each group. (B). Quantitative analysis results from micro-CT evaluation. BV/TV = the bone volume/total volume; Tb.Th = the mean trabecular thickness; Tb.sp = trabecular spacing; Tb.N = trabecular number *$P < 0.05$.

Conclusions

Forsythiaside inhibited the osteoclastogenesis while inhibiting the particle-induced inflammation, resulting in a decreased secretion of inflammatory cytokines, such as TNF-α, IL-1β, and inflammation-induced osteoclastogenesis. Moreover, forsythiaside could inhibit RANKL-induced osteoclastogenesis and Ti particle-induced periprosthetic osteolysis *via* the ERK, JNK, and p38 signaling pathways. These biofunctions of forsythiaside contributed to the implant-associated particle-induced osteolysis. Thus, forsythiaside can act as a candidate for the precaution of implant-associated particle-induced osteolysis.

Statement

All experiments were performed in compliance with relevant laws or guidelines and all experiments followed institutional guidelines. All animal procedures were performed in accordance with the Guidelines for Care and Use of Laboratory Animals of Navy Military Medical University and approved by the Animal Ethics Committee of Shanghai Changhai Hospital, China.

Conflicts of interest

There are no conflicts to declare.

Acknowledgements

This work was supported by the grants received from the Shanghai Committee of Science and Technology Foundation (No. 13411951500) and The Second Military Medical University School Program (2016QN09).

References

1 Y. Jiang, T. Jia, P. H. Wooley and S.-Y. Yang, *Acta Orthop. Belg.*, 2013, **79**, 1–9.
2 J. Gallo, J. Vaculova, S. B. Goodman, Y. T. Konttinen and J. P. Thyssen, *Acta Biomater.*, 2014, **10**, 2354–2366.
3 X. Liu, X. Qu, C. Wu, Z. Zhai, B. Tian, H. Li, Z. Ouyang, X. Xu, W. Wang, Q. Fan, T. Tang, A. Qin and K. Dai, *Biomaterials*, 2014, **35**, 5721–5730.
4 Z. Ouyang, Z. Zhai, H. Li, X. Liu, X. Qu, X. Li, Q. Fan, T. Tang, A. Qin and K. Dai, *Biochem. Pharmacol.*, 2014, **90**, 276–287.
5 F. Liu, Z. Zhu, Y. Mao, M. Liu, T. Tang and S. Qiu, *Biomaterials*, 2009, **30**, 1756–1762.
6 Y. T. Tai, C. Acharya, G. An, M. Moschetta, M. Y. Zhong, X. Feng, M. Cea, A. Cagnetta, K. Wen, H. van Eenennaam, A. van Elsas, L. Qiu, P. Richardson, N. Munshi and K. C. Anderson, *Blood*, 2016, **127**, 3225–3236.
7 S. Harshan, P. Dey and S. Ragunathan, *PeerJ*, 2018, **6**, e5743.
8 J. Ma, Y. Ma, X. Liu, S. Chen, C. Liu, A. Qin and S. Fan, *Biochem. J.*, 2015, **469**, 399–408.
9 Z. J. Zhai, H. W. Li, G. W. Liu, X. H. Qu, B. Tian, W. Yan, Z. Lin, T. T. Tang, A. Qin and K. R. Dai, *Br. J. Pharmacol.*, 2014, **171**, 663–675.
10 X. Qu, J. Mei, Z. Yu, Z. Zhai, H. Qiao and K. Dai, *Biochem. Biophys. Res. Commun.*, 2018, **501**, 547–555.
11 J. Wang, X. Wu and Y. Duan, *Front. Pharmacol.*, 2018, **9**, 64.
12 J. Wang, Y. Tao, Z. Ping, W. Zhang, X. Hu, Y. Wang, L. Wang, J. Shi, X. Wu, H. Yang, Y. Xu and D. Geng, *Sci. Rep.*, 2016, **6**, 23827.
13 Z. Ping, Z. Wang, J. Shi, L. Wang, X. Guo, W. Zhou, X. Hu, X. Wu, Y. Liu, W. Zhang, H. Yang, Y. Xu, Y. Gu and D. Geng, *Acta Biomater.*, 2017, **62**, 362–371.

14 Z. Ping, X. Hu, L. Wang, J. Shi, Y. Tao, X. Wu, Z. Hou, X. Guo, W. Zhang, H. Yang, Y. Xu, Z. Wang and D. Geng, *Acta Biomater.*, 2017, **51**, 513–525.
15 C. Wu, W. Wang, B. Tian, X. Liu, X. Qu, Z. Zhai, H. Li, F. Liu, Q. Fan and T. Tang, *Biochem. Pharmacol.*, 2015, **93**, 59–71.
16 H. Qu, Y. Zhang, Y. Wang, B. Li and W. Sun, *J. Pharm. Pharmacol.*, 2008, **60**, 261–266.
17 J. Qian, X. Ma, Y. Xun and L. Pan, *Eur. J. Pharmacol.*, 2017, **812**, 250–255.
18 H. Li, D. Tang, C. Qi, X. Zhao, G. Wang, Y. Zhang and T. Yu, *J. Orthop. Surg. Res.*, 2018, **13**, 139.
19 H. Qu, Y. Zhang, X. Chai and W. Sun, *Bioorg. Chem.*, 2012, **40**, 87–91.
20 X.-Y. Zeng, W. Yuan, L. Zhou, S.-X. Wang, Y. Xie and Y.-J. Fu, Forsythoside A exerts an anti-endotoxin effect by blocking the LPS/TLR4 signaling pathway and inhibiting Tregs in vitro, *Int. J. Mol. Med.*, 2017, **40**(1), 243–250.
21 Y. Jiang, T. Jia, P. H. Wooley and S. Y. Yang, *Acta Orthop. Belg.*, 2013, **79**, 1–9.
22 E. Jamsen, V. P. Kouri, M. Ainola, S. B. Goodman, D. C. Nordstrom, K. K. Eklund and J. Pajarinen, *J. Biomed. Mater. Res., Part A*, 2017, **105**, 454–463.
23 S. Landgraeber, M. Jäger, J. J. Jacobs and N. J. Hallab, *Mediators Inflammation*, 2014, **2014**, 185150.
24 N. J. Hallab and J. J. Jacobs, *Front. Endocrinol.*, 2017, **8**, 5.
25 G. Cheng, Y. Zhao, H. Li, Y. Wu, X. Li, Q. Han, C. Dai and Y. Li, *Exp. Ther. Med.*, 2014, **7**, 179–184.
26 H. Li, D. Tang, C. Qi, X. Zhao, G. Wang, Y. Zhang and T. Yu, *J. Orthop. Surg. Res.*, 2018, **13**, 139.
27 W. J. Boyle, W. S. Simonet and D. L. Lacey, *Nature*, 2003, **423**, 337–342.